iScience

CellPress
OPEN ACCESS

Article

Inhibition of HIV-1 replication by nanobodies targeting tetraspanin CD9

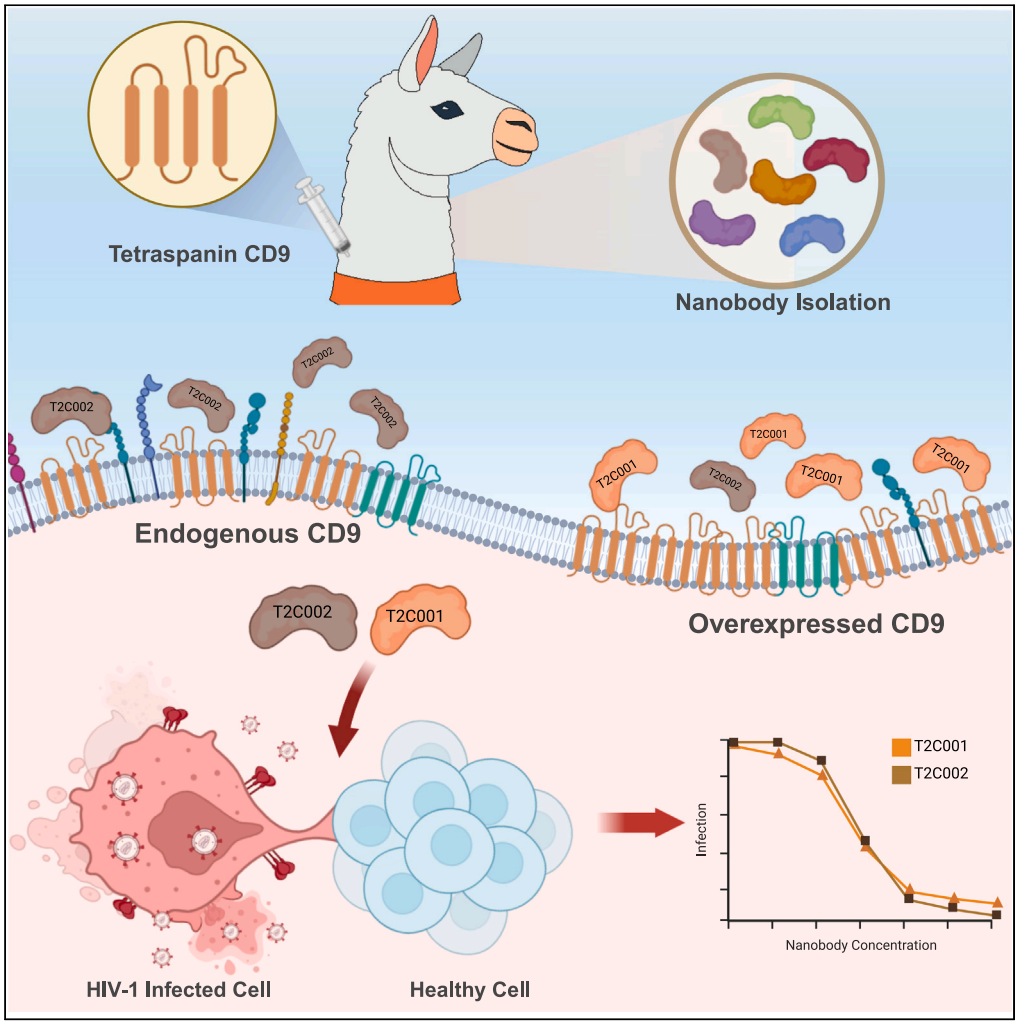

Jeffrey C. Umotoy, Pascal Z. Kroon, Shirley Man, ..., Neeltje A. Kootstra, Marit J. van Gils, Steven W. de Taeye

j.c.umotoy@amsterdamumc.nl (J.C.U.)
s.w.detaeye@amsterdamumc.nl (S.W.d.T.)

Highlights

Nanobodies targeting CD9 large extracellular loop isolated through llama immunization

T2C001 and T2C002 recognize endogenous and overexpressed CD9 on the cell surface

Nanobodies did not inhibit the early stages of HIV-1 infection

T2C001 and T2C002 prevented HIV-1 replication and syncytia formation

Umotoy et al., iScience 27, 110958
October 18, 2024
https://doi.org/10.1016/j.isci.2024.110958

iScience

CellPress
OPEN ACCESS

Article

Inhibition of HIV-1 replication by nanobodies targeting tetraspanin CD9

Jeffrey C. Umotoy,[1,3,*] Pascal Z. Kroon,[1,3,5] Shirley Man,[2,3,5] Karel A. van Dort,[2,3] Tugba Atabey,[1,3] Angela I. Schriek,[1,3] Gillian Dekkers,[4] Elena Herrera-Carrillo,[1,3] Teunis B.H. Geijtenbeek,[2,3] Raimond Heukers,[4] Neeltje A. Kootstra,[2,3] Marit J. van Gils,[1,3] and Steven W. de Taeye[1,3,6,*]

SUMMARY

HIV-1 alters the dynamics and distribution of tetraspanins, a group of proteins integral to membrane organization, to facilitate both entry and egress. Notably, the tetraspanin CD9 is dysregulated during HIV-1 infection, correlating with multifaceted effects on viral replication. Here, we generated llama-derived nanobodies against CD9 to restrict HIV-1 replication. We immunized llamas with recombinant large extracellular loop of CD9 and identified eight clonally distinct nanobodies targeting CD9, each exhibiting a range of affinities and differential binding to cell surface-expressed CD9. Notably, nanobodies T2C001 and T2C002 demonstrated low nanomolar affinities and exhibited differential sensitivities against endogenous and overexpressed CD9 on the cell surface. Although CD9-directed nanobodies did not impede the early stages of HIV-1 life cycle, they effectively inhibited virus-induced syncytia formation and virus replication in T cells and monocyte-derived macrophages. This discovery opens new avenues for host-targeted therapeutic strategies, potentially augmenting existing antiretroviral treatments for HIV-1.

INTRODUCTION

Forty years since the identification of HIV-1 as the causative agent for AIDS, HIV-1 remains as a global health challenge, necessitating a continuous advancement in therapeutic strategies to achieve an ultimate cure. Antiretroviral therapy (ART), which played an effective role in controlling viral replication, primarily focuses on targeting viral components to inhibit replication but often fall short in eradicating the latent viral reservoirs. Host-targeting strategies, particularly utilizing antibodies, present a paradigm shift by directing the immune response toward essential host factors involved in the HIV-1 replication cycle. Moreover, targeting host factors has the potential to exhibit a broad spectrum of activity and may overcome challenges associated with viral diversity and mutational escape.[1] Antibody-based host-targeting strategies may also reduce the risk of developing resistance to direct-acting ART as these host targets are conserved, essential for viral replication, and are most likely present in cells harboring latent HIV-1. Additionally, these host-targeting strategies have the potential to act in synergy with HIV-specific broadly neutralizing antibodies or ART.

CD9, a member of the tetraspanin family, has emerged as a therapeutic target in viral infection because of its involvement in the process of cell fusion. Tetraspanins act as master organizers of the plasma cell membrane by facilitating clustering of proteins and protein partners and offer a spatiotemporal location required for physiological function.[2,3] This family of proteins can associate with integrins, immunoglobulins, proteases, and other members of the tetraspanin family forming complex protein networks called tetraspanin-enriched microdomains (TEMs).[2,4] They are involved in many cellular processes including intercellular signaling, proliferation, migration, adhesion, and fusion (reviewed in the study by Reyes et al.[5]). CD9-deficient mice had impaired fertilization due to the inhibition of egg-sperm fusion.[6,7] Additionally, CD9 is involved in canine distemper virus uptake,[8] entry of coronaviruses and influenza virus,[9,10] and modulation of human papilloma virus.[11] Aberrant CD9 function is linked to pathological processes in tumorigenesis, metastasis, and viral and bacterial infection.[3,12,13]

HIV-1 is known to exit at sites on the plasma membrane that are highly enriched in tetraspanins.[14] Tetraspanins have been shown to colocalize with both HIV-1 Env and Gag proteins in T cells, dendritic cells, and macrophages.[15–20] Furthermore, tetraspanins are incorporated into HIV-1 particles to facilitate release from infected cells,[21] and HIV-1 accessory proteins Vpu and Nef are able to directly regulate tetraspanin expression on the cell surface.[22,23] In a recent study performed in our group, Kruize and colleagues found that CD9 is upregulated upon HIV-1 infection of macrophage and can support viral replication. Subsequently, downregulation of CD9 decreased HIV-1 replication.[24]

[1]Department of Medical Microbiology and Infection Prevention, Amsterdam University Medical Center (UMC), University of Amsterdam, Amsterdam, the Netherlands
[2]Department of Experimental Immunology, Amsterdam UMC, University of Amsterdam, Amsterdam, the Netherlands
[3]Amsterdam Institute for Immunology and Infectious Diseases, Amsterdam, the Netherlands
[4]QVQ Holding BV, Yalelaan 1, 3584 CL Utrecht, the Netherlands
[5]These authors contributed equally
[6]Lead contact
*Correspondence: j.c.umotoy@amsterdamumc.nl (J.C.U.), s.w.detaeye@amsterdamumc.nl (S.W.d.T.)
https://doi.org/10.1016/j.isci.2024.110958

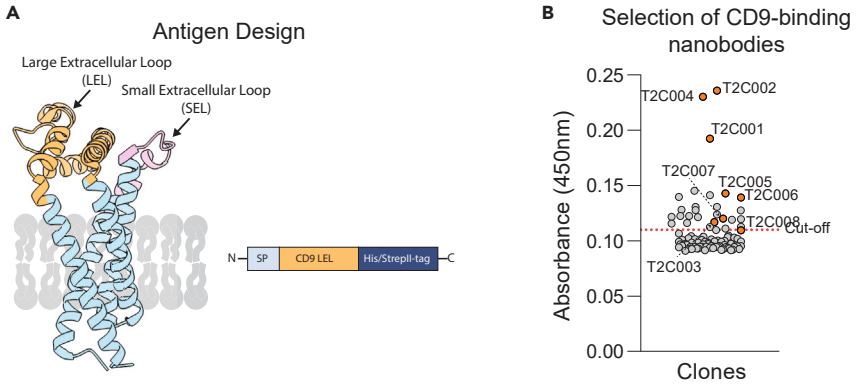

Figure 1. Antigen design and selection

(A) Structural representation of full-length CD9 with transmembrane domains (light blue), large extracellular loop (LEL) (yellow), and small extracellular loop (pink). CD9 LEL (AA 112–195, Uniprot, P21926) is cloned into a mammalian expression plasmid flanked by a signal peptide (SP) and purification tag (6× His-tag or Strep-tag II).

(B) ELISA binding data from periplasmic fraction-containing nanobodies against CD9 LEL measured at OD490 nm. An arbitrary cutoff signal of 0.11 nm (red dashed line) was generated to select for clones with high binding to CD9 LEL. Clones in orange correspond to unique clones tested further downstream.

This work describes the development and characterization of CD9-directed nanobodies and explored their potential inhibitory effect against HIV-1 replication. Llama immunization with CD9 large extracellular loop (LEL) resulted in the isolation of clones of varying affinities and cell-binding properties. Additionally, CD9-directed nanobodies exhibited distinctive sensitivities against surface-expressed CD9 with differential binding to endogenous and overexpressed CD9. When tested for their inhibitory role in HIV-1 infection, CD9-directed nanobodies significantly inhibited cell-cell spread of infection and HIV-1 replication in T cells and macrophages.

RESULTS

Recombinant CD9 LEL induced humoral response in *Llama glama* after immunization

To obtain nanobodies targeting CD9, two *Llama glama* (llamas) were immunized with recombinant CD9 LEL produced as a soluble protein (Figure 1A). CD9 LEL was chosen as the immunogen because of its implication in molecular associations with partner proteins.[25] Affinity purification and two rounds of size-exclusion chromatography produced a monomeric 11-kDa protein validated by SDS-PAGE, with a total production yield of 4 mg/L (Figures S1A and S1B). To confirm proper protein folding of CD9 LEL, we performed an ELISA and western blot analysis with a monoclonal antibody validated to recognize CD9 (Figures S1B and S1C).

Llamas were immunized with CD9 LEL and humoral immune response toward CD9 LEL was followed by ELISA (Figures S2A and S2B). Subsequently, nanobody phage display libraries were constructed using PCR amplification from total peripheral blood mononuclear cell (PBMC) RNA. The final libraries contained ~10^9 transformants. High-affinity nanobodies were enriched by two rounds of biopanning on decreasing amounts of immobilized CD9 LEL. From the outputs, 92 single colonies were subsequently picked and expressed in *E. coli* periplasm for further testing (Figure 1B).

CD9-binding nanobodies have high sequence diversity and varying affinities

Periplasmic fraction-containing nanobodies were tested for binding against CD9 LEL by ELISA. This selection round resulted in 15 clones with reactivity against CD9 LEL that fulfilled an arbitrary cutoff signal of OD490 nm = 0.11 nm (Figure 1B). Subsequent sequencing of the enriched clones identified 8 unique clusters based on the homology in the CDR3 sequence. CDR3 length varied from 12 amino acids to 22 amino acids, with 3 clones bearing 17 amino acids in the CDR3, which falls within the normal CDR3 lengths of nanobodies[26] (Figure S3). Multiple sequence alignment of the top eight clones revealed homology between 14.3% and 50% based on their CDR3 (Figure 2A). The 8 unique clones were produced to high purity and validated by SDS-PAGE and Coomassie staining (Figure 2B). A band corresponding to the nanobody was visible at ~16 kDa for all clones, with some clones showing two visible bands (T2C003 and T2C006). The presence of other bands likely consists of nanobodies in which the C-terminal tag has been partially cleaved off. Multiple bands have been previously observed in other nanobodies.[27] All nanobodies, except T2C004, were purified to a relatively good yield.

We next assessed the binding affinities of the nanobodies by ELISA and biolayer interferometry (BLI). The different clones revealed varying affinities to CD9 LEL by ELISA from low nanomolar affinity to several clones not achieving an affinity at >1,000 nM (Table 1). Clones with the highest apparent binding affinities were T2C001 and T2C002, with affinities of 2.73 and 16.9 nM, respectively (Figure 2C). We then determined the binding kinetics of the nanobodies by BLI. We observed dissociation constant (K_D) values in the nanomolar range for T2C001 and T2C002 (3.0×10^{-9} M and 7.6×10^{-9} M, respectively), and one magnitude lower K_D value for the rest of the clones, while K_D values is too low to be determined for T2C007 and T2C008 (Table 1). Overall, binding affinities and kinetics as measured by ELISA and BLI aligned well with T2C001

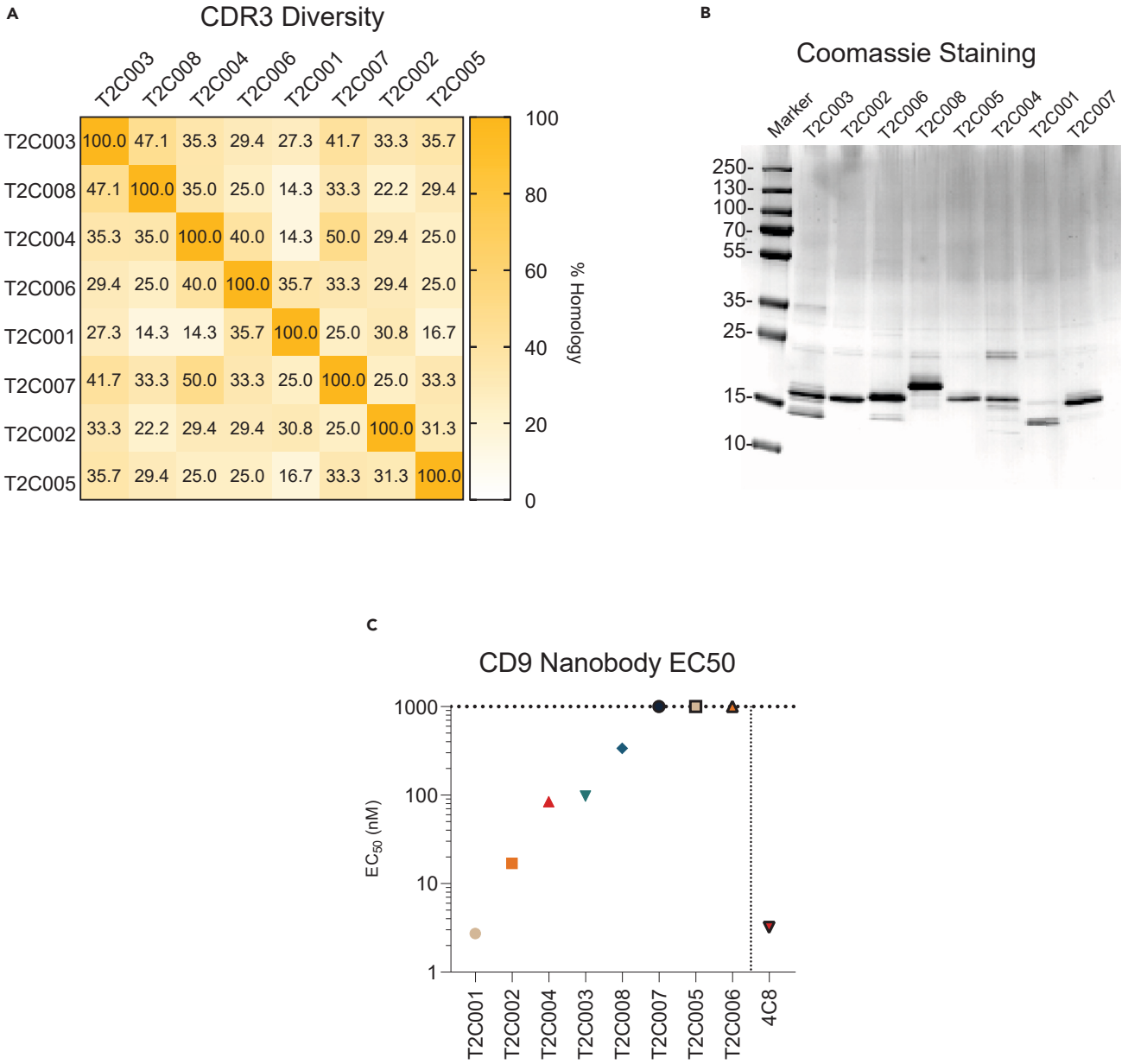

Figure 2. Characterization of CD9-directed nanobodies

(A) Multiple sequence analysis of CD9-directed nanobodies with unique sequences based on their similarities on CDR3 (percent homology).

(B) SDS-PAGE and Coomassie staining of eight nanobody clones.

(C) CD9-directed nanobodies affinity as measured by ELISA. CD9 LEL was immobilized on high-binding ELISA plates followed by dilution of CD9 nanobodies to determine binding affinity. This includes a published CD9 nanobody, 4C8.

and T2C002 consistently showing high binding toward CD9 LEL. No apparent cross-reactivity was observed against CD81-Fc by ELISA, which shares high homology to CD9 (Figure S4).[25,28] These data highlight the isolation of specific and high-affinity nanobodies against CD9.

Comparative analysis of CD9 nanobodies against previously published 4C8

Oosterheert and colleagues solved the structure of CD9 in complex with 4C8, a CD9-directed nanobody, and EWI-F, CD9's primary protein partner.[29,30] They found the epitope of 4C8 to be located in the CD9 LEL, which could form a 4C8-CD9 LEL-EWI-F complex. Since our immunogen is based on CD9 LEL, we explored any possible similarities in binding and epitope targeted by our CD9-directed nanobodies to 4C8. We produced 4C8 to high purity and compared its binding affinity to T2C001 and T2C002 by ELISA. 4C8 exhibited an affinity of 3.21 nM against CD9 LEL, which is in a similar nanomolar range as T2C002 and T2C001 (Figure 2C). Additionally, multiple sequence alignment

Table 1. Characterization of CD9 nanobodies by Octet (K_D) and ELISA (affinity)

Clones	K_D (M)	ka (1/ms)	kdis (1/s)	Affinity (nM)
T2C001	3.03E−09	9.48E+05	2.87E−03	2.72
T2C002	7.57E−09	2.11E+05	1.60E−03	16.9
T2C003	1.32E−08	6.16E+05	8.10E−03	97.44
T2C004	3.60E−08	1.36E+06	4.90E−02	84.33
T2C005	5.25E−08	5.01E+04	2.63E−03	>1,000
T2C006	8.28E−08	6.84E+04	5.66E−03	>1,000
T2C007	1.00E−07	1.00E+04	1.00E−03	>1,000
T2C008	6.64E−06	3.68E+03	2.44E−02	338.6

ka, on rates; kdis, off rates.

also revealed high homology between 4C8 and T2C002 (42.9%) in CDR3 (Figure 3A). Furthermore, arginine residue (R101) in the CDR3 of 4C8 forms a salt bridge with E160 on CD9 LEL, alongside two tryptophan (W53 of CDR2 and W102 of CDR3) forming a hydrophobic core in the interface of CD9 LEL as key for 4C8-CD9 complex (Figure 3B). This R101 residue is conserved in T2C002 and the tryptophan is also conserved in several more clones in our panel. Superimposing the *in-silico*-predicted structure of the nanobodies with the solved structure of 4C8 and CD9 LEL (PDB: 6Z1V) showed similar CDR3 orientation and approach to the binding groove on CD9 LEL for T2C002 and T2C007, while T2C001 has little overlap to the binding groove compared to the rest of the nanobodies with CDR3 pointing at a different orientation (Figure 3C). Thus, T2C002 may have similar binding homology to 4C8 based on its similarities in CDR3 sequence, affinity, and the conservation of contact residues to CD9; nonetheless, structural studies are needed to determine the exact epitope of our CD9-targeting nanobodies.

CD9-directed nanobodies have variable recognition of CD9 on cells

Next, we evaluated the capacity of CD9-directed nanobodies to bind cell surface-expressed CD9 in a panel of cell lines with endogenous CD9 expression (HEK293T, HeLa, and SupT1) or lacking CD9 expression (Raji)[31] (Figures S5A–S5C). We observed that the highest affinity clone, T2C002, showed strong binding across all cell lines tested (Figures 2D and S5B). Notably, T2C007, despite its low affinity for CD9 LEL protein (affinity >1,000 nM), demonstrated the most pronounced binding across all tested cell lines. This nanobody also exhibited less variability in CD9 recognition on different cell lines compared to T2C002. Additionally, T2C004 bound to cells, though with significantly lower affinity. In contrast, no binding was detected for nanobodies T2C003, T2C006, T2C008, T2C005, and particularly T2C001, which exhibited remarkable affinity to CD9 LEL. As expected, no binding was observed to CD9-deficient Raji cells.

Moreover, we overexpressed full-length CD9 on HEK293T cells to determine whether the panel of CD9-directed nanobodies is sensitive to antigen density on the cell surface. We verified CD9 overexpression via flow cytometry (HI9a, BioLegend) (Figure 4A). Interestingly, overexpressed CD9 led to a substantial increase in binding (from background level binding to 26% of cells) by the previously non-binding T2C001 (Figure S5B). The binding of T2C002 and T2C001 in overexpressed CD9 seemed to be preserved.

These cell-binding data suggest that CD9-directed nanobodies have different binding properties on CD9 expressed on the cell surface, recognize distinct epitopes and/or confirmation, and have cell type-specific variations. Additionally, T2C001 seemed to recognize CD9 conformation only present in CD9 overexpressed on the cell surface.

Differential binding of T2C001 and T2C002 to endogenous vs. overexpressed CD9

We further characterized T2C001 and T2C002 because of their contrasting cell-binding feature. We serially diluted T2C001 and T2C002 and tested their binding to wild-type HEK293T cells, CD9-transfected HEK293T cells, and SupT1 (Figures 4A and S5D). Flow cytometry analysis revealed distinct binding profiles for the two nanobodies (Figure 4B). T2C002 bound wild-type HEK293T cells and SupT1 cells in a dose-dependent manner, while T2C001 exhibited minimal binding. Overexpression of CD9 in HEK293T cells led to a marked increase in binding for both T2C001 and T2C002, with T2C001 showing a more pronounced increase in the percentage of positive cells.

Examining the flow cytometry plot reveals that T2C002 seemed to recognize and bind endogenous CD9 across a larger proportion of cells in wild-type HEK293T cells (Figure 4C), while T2C001 seemed to recognize only the exogenous overexpressed CD9. Furthermore, T2C002 is also able to bind exogenous CD9, albeit exhibiting nonidentical binding pattern than T2C001, with either nanobodies binding to different cell subpopulation. This is best visualized by flow cytometry histogram (Figure 4D).

To determine if the level of CD9 overexpression affects the recognition of CD9-directed nanobodies, we transfected HEK293T cells with varying concentrations of CD9 full-length DNA (5 μg, 20 μg, 40 μg, or mock). Flow cytometry analysis confirmed overexpression of CD9 in comparison to wild-type HEK293T cells (Figure 4A). CD9 transfection reveals a characteristic two subpopulation – a smaller frequency lower peak and a larger frequency higher peak, as evident in the flow cytometry histogram overlay. Furthermore, there is a dose-dependent increase in CD9 expression with increasing concentration of exogenous CD9. Binding of the nanobodies reveals that increased overexpression of CD9 did not have an effect on the binding of T2C002, while T2C001 exhibited a stronger response to increasing CD9 levels, indicating potential positive dependence on CD9 density on the cell surface.

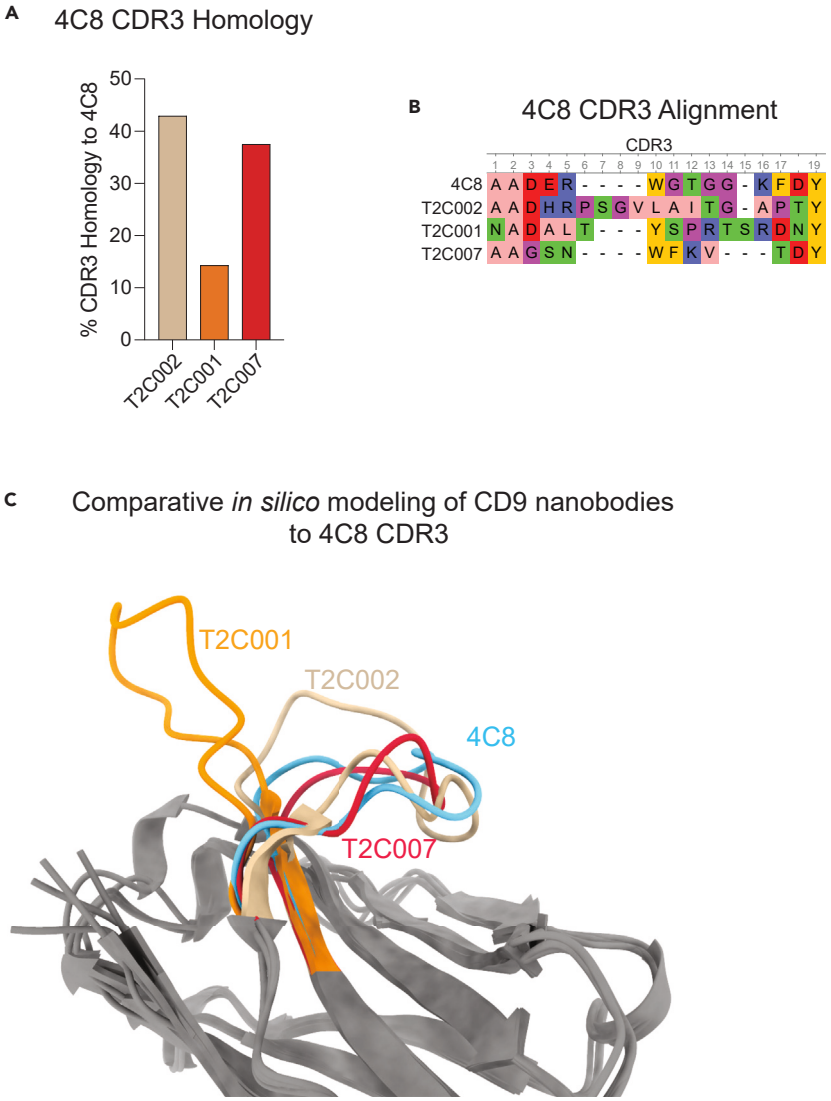

Figure 3. Comparison to 4C8

(A) Percent homology and sequence alignment (B) of the CDR3 of T2C001, T2C002, and T2C007 with the published nanobody, 4C8.

(C) *In silico* superimposition of the predicted structures of T2C001, T2C002, and T2C007 to the solved crystal structure of 4C8 in complex with CD9 (obtained from PDB: 6Z1V). Separate colors are used to depict the CDR3 regions of individual nanobody predictions in comparison to 4C8 CDRH3. The rest of the predicted nanobody structure is colored in gray.

Early stages of HIV-1 replication are not inhibited by CD9-directed nanobodies

To evaluate the inhibitory effect of nanobodies targeting CD9 on the early stages of HIV-1 infection, we performed a TZM-bl assay.[32] Nanobody J3, a broad and potent HIV-1 Env-targeting nanobody, was used as a positive control. Incubation of TZM-bl cells with J3 prior to the addition of the virus exhibited a potent inhibitory effect on HIV-1 infection in a dose-dependent manner (Figure 5A). In contrast, the CD9-directed nanobodies tested (T2C001, T2C002, and T2C007) did not inhibit the early stages of HIV-1 infection across the range of concentrations tested. These findings indicate that CD9 blockade by nanobodies does not impact the early stages of HIV-1 infection as measured by the TZM-bl assay.

Cell-cell transmission of HIV-1 is blocked by CD9-directed nanobodies

The cell-to-cell spread of HIV-1 is an important route of virus transmission, and to determine whether blocking with nanobodies could disrupt this process, we analyzed syncytia formation of infected SupT1 cells by microscopy 4 days post infection in the absence or presence of CD9-directed nanobodies (Figure 5B). Syncytia were graded based on the number of multinucleated cells, cytopathic effect, total cell death, and

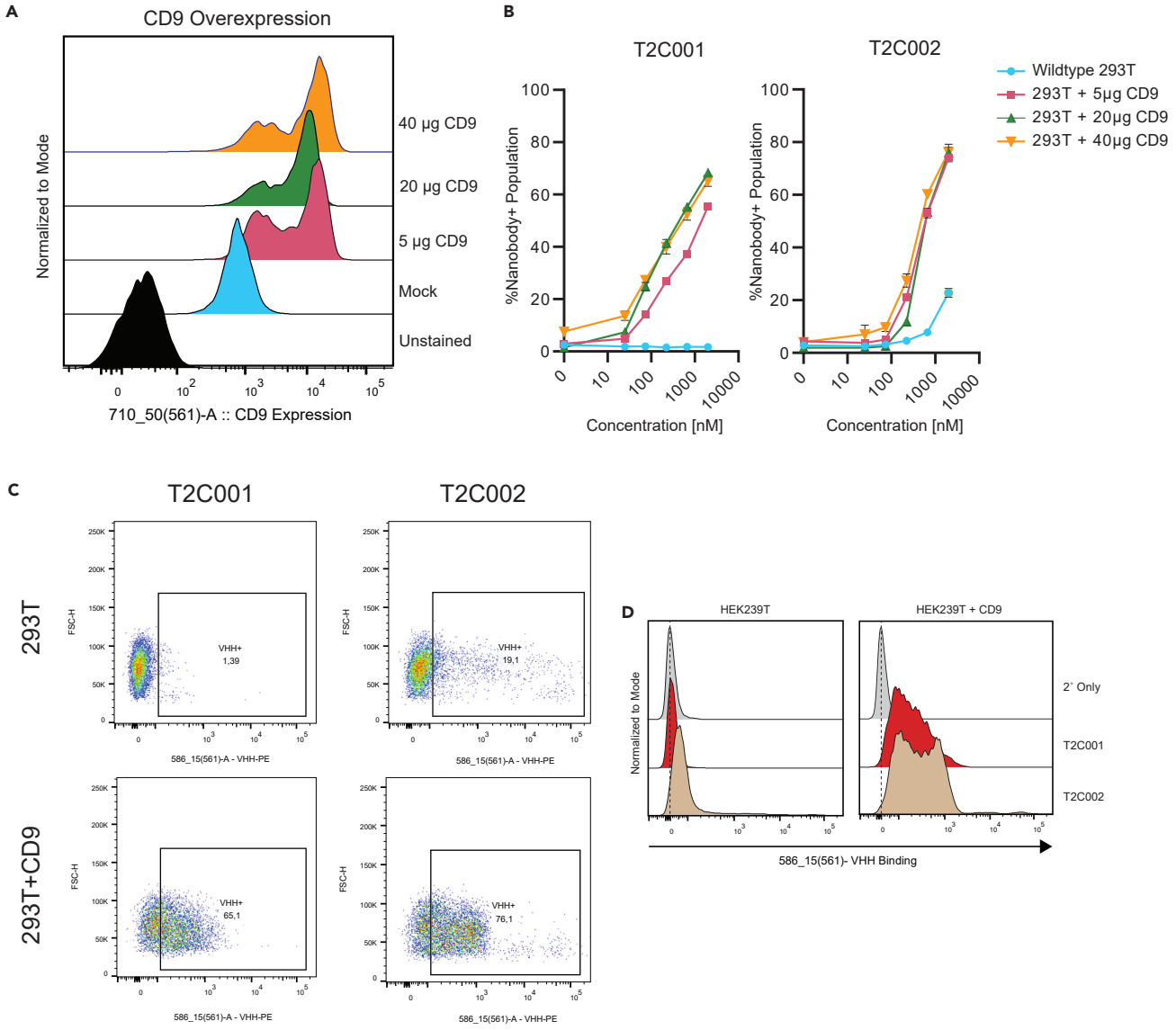

Figure 4. Cell-binding characterization of T2C001 and T2C002

(A) Flow cytometry histogram of CD9 expression on wild-type (WT) HEK293T cells and HEK293T transfected with different concentration of full-length CD9 DNA. Signal was detected using a primary anti-CD9 PerCP/Cyanine5.5 (BioLegend).

(B) Determination of cell-binding affinity of T2C001 and T2C002 on WT HEK293T and HEK293T cells transfected with different concentration of full-length CD9. Nanobody binding was detected by MonoRab Rabbit Anti-Camelid VHH Cocktail (PE). Percent positive population was determined.

(C) Flow cytometry plot and histogram (D) of T2C001 and T2C002 binding to WT HEK293T cells and CD9-transfected HEK293T cells. Nanobody binding was detected by MonoRab Rabbit Anti-Camelid VHH Cocktail (PE).

opacity, as detailed in the STAR methods section (visualized in Figure S7). J3 nanobody was used as a positive control, which besides its potency in neutralizing viral particles, also exhibited efficient neutralization of HIV-1 cell-cell spread.[33]

Our results show a dose-dependent inhibition of syncytia formation with nanobody J3 treatment resulting in complete inhibition at 100 and 1,000 nM. Similar dose-dependent inhibitory effects were observed with T2C002, T2C001, and T2C007, although with less potency. A CD9 monoclonal antibody (mAb) (Sino Biological) also demonstrated syncytia inhibition. Intriguingly, a combined treatment of nanobody J3 and T2C002 resulted in an additive inhibitory effect. As a negative control, T2C004 CD9-directed clone, which lacks binding of CD9 on the cell surface, was included. This clone did not elicit any inhibitory role in the formation of syncytia. Our finding suggests that blocking CD9 could play a significant role in hindering the formation of syncytia and thus inhibiting cell-to-cell transmission, thereby potentially disrupting a key pathway in HIV-1 dissemination.

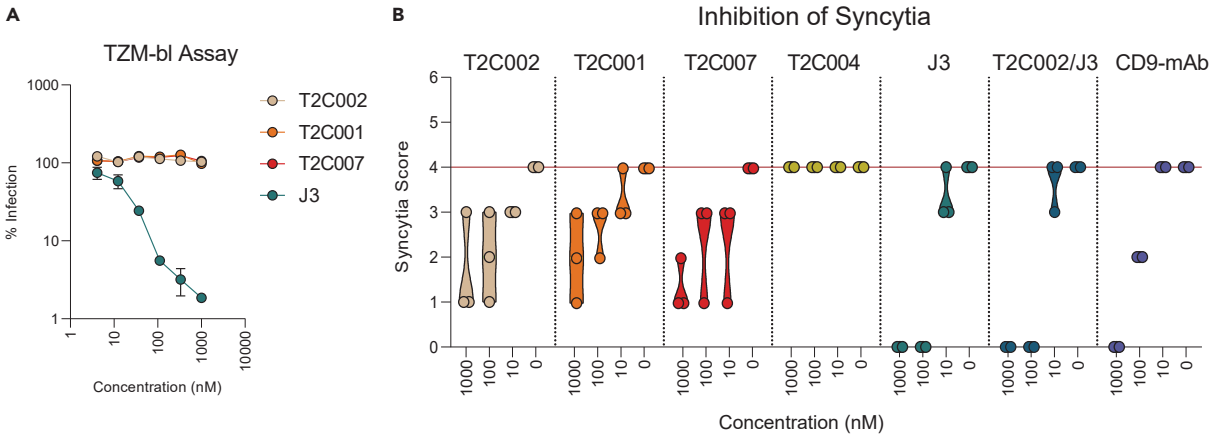
A
TZM-bl Assay
% Infection
Concentration (nM)
T2C002
T2C001
T2C007
J3
B
Inhibition of Syncytia
T2C002
T2C001
T2C007
T2C004
J3
T2C002/J3
CD9-mAb
Syncytia Score
Concentration (nM)

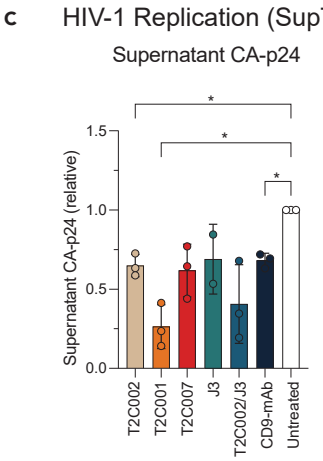
C
HIV-1 Replication (SupT1)
Supernatant CA-p24
Supernatant CA-p24 (relative)
T2C002
T2C001
T2C007
J3
T2C002/J3
CD9-mAb
Untreated

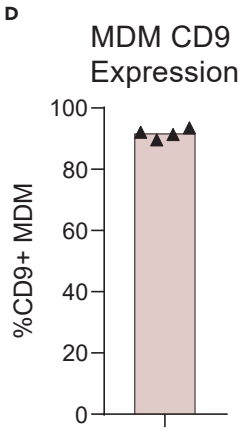
D
MDM CD9
Expression
%CD9+ MDM

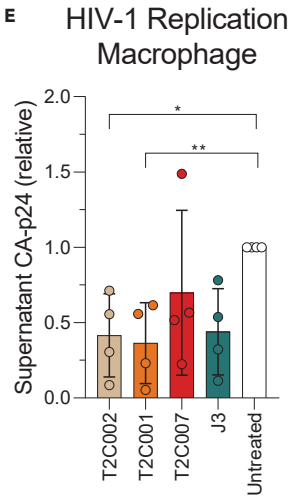
E
HIV-1 Replication
Macrophage
Supernatant CA-p24 (relative)
T2C002
T2C001
T2C007
J3
Untreated

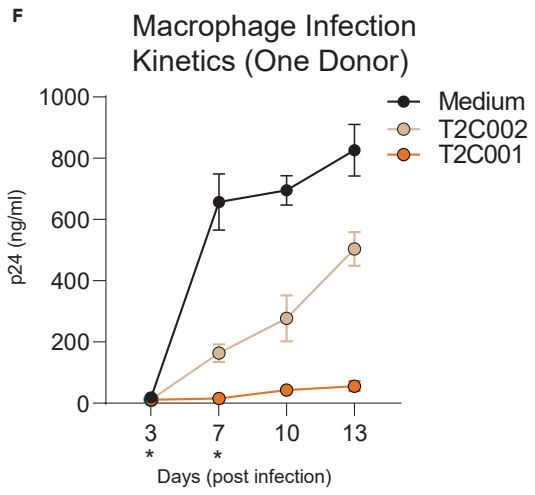
F
Macrophage Infection
Kinetics (One Donor)
Medium
T2C002
T2C001
p24 (ng/ml)
Days (post infection)

Figure 5. Effect on HIV-1 replication

(A) TZM-bl assay. TZM-bl cells were incubated with a serial dilution of nanobodies prior to infection with BG505 infectious molecular clone. Virus entry is measured by TZM-bl luciferase signal. Data are presented as percent infection. J3 is used as a positive control.

(B) Inhibition of HIV-1-induced syncytia in T cells measured by syncytia scoring. SupT1 cells were treated with nanobodies prior to infection with HIV LAI (MOI 0.15) and cultured for 3 days post infection. Syncytia score 6 = zero live cells with large opaque multi-nucleated cells, score 0 = all viable cells. Scoring was performed when negative control reaches syncytia score of 4. Each condition was performed in triplicates. Media-only condition served as no treatment control, media plus virus as reference control, and a CD4-binding site nanobody, J3, as a positive control. Additionally, a condition with CD9 mAb treatment was included.

(C) Inhibition of HIV-1 replication. SupT1 cells were treated with nanobodies prior to infection with HIV LAI (MOI 0.15), and CA-p24 was measured by an in-house ELISA in the supernatant at day 3 post infection as a measure of viral release.

(D) CD9 surface expression on MDM by flow cytometry from four different donor PBMCs. An isotype control was included to determine non-specific binding signal.

(E) Inhibitory effect of nanobodies on HIV-1 replication on macrophage. MDMs were infected with HIV-1 NL4-3 BaL. Nanobodies (0.1 μM) were added on day 3 post infection. HIV-1 replication is measured by CA-p24 levels in the supernatant day 7 posy infection. Mean ± SD of 4 replicates from different MDM donors is shown. Paired groupwise comparisons were performed using Friedman's ANOVA. A p value of <0.05 was considered statistically significant.

(F) Inhibitory effect of CD9-directed nanobodies on HIV-1 replication in MDM over time. CA-p24 levels in the supernatant were determined for days 3, 7, 10, and 13 post infection, with medium as a positive control. A representative donor is shown.

Effect of CD9-directed nanobodies on HIV-1 replication

Given the existing evidence that antibody-mediated blockade of CD9 can inhibit the viral release of HIV-1 and other viruses,[34–36] our study aimed to assess whether a similar inhibitory effect on HIV-1 replication could be achieved through a nanobody-based approach directed to CD9. To this end, we determined CA-p24 in the culture supernatant of infected SupT1 cells 4 days post infection (Figures 5C and S6). HIV-1 infection of SupT1 markedly increased CD9 expression (Figure S8). Treatment with T2C002 and T2C001 markedly reduced CA-p24 levels in the supernatant, potentially inhibiting viral release. Additionally, treatment with CD9 mAb significantly reduced CA-p24 levels in the supernatant, even at a 4-fold lower concentration tested (250 nM for CD9 mAb vs. 1,000 nM for nanobodies). Collectively, these results underscore the potential of CD9-directed nanobodies as a novel host-targeting strategy to inhibit HIV-1 replication.

Viral egress is inhibited by CD9 nanobodies in macrophages

Macrophages are considered important in the establishment and persistence of the HIV-1 reservoir, and shRNA-mediated downregulation of CD9 significantly decreases HIV-1 egress from infected monocyte-derived macrophages (MDMs).[24] Therefore, we extended the evaluation of CD9-directed nanobodies to limiting HIV-1 infection in macrophages. After verifying CD9 expression on the cell surface (Figures 5D and S9), MDMs obtained from four different donors were infected with NL4-3 BaL, and subsequently, CD9-directed nanobodies were added to the cultures. CA-p24 levels in the supernatant were quantified as a measure of viral release. Our results indicated a significant reduction in viral release when infected MDMs were treated with T2C002 and T2C001, compared to untreated controls (Figure 5E). A reduction in viral release was also observed with nanobody J3, albeit not reaching statistical significance. Furthermore, the inhibitory effect of CD9-directed nanobodies was observed overtime maintaining reduced CA-p24 levels in the supernatant (Figure 5F). These results suggest that nanobody-based blockage of CD9 may be an effective strategy in reducing HIV-1 replication, akin to the effects observed with shRNA-mediated CD9 downregulation.

DISCUSSION

This work describes the successful generation of CD9-directed nanobodies through immunization of llama, demonstrating varied affinities and specificities to cell surface-expressed CD9, and offers a promising therapeutic approach against HIV-1 replication. One clone, T2C001, exhibited dramatic preference for overexpressed CD9 on the cell surface, while other clones (T2C002 and T2C007) seemed to have less variability in the recognition of CD9 on the cell surface. *In silico* modeling, multiple sequence analysis, and binding of these clones revealed possible epitope overlaps with 4C8, a CD9-targeting nanobody with a solved structure in complex with CD9. Treatment of HIV-1-infected T cells and macrophages with the nanobodies significantly reduced viral replication as observed with the reduction in viral release and inhibition of syncytia, but did not have an effect on the early stages of viral replication.

The CD9-targeting nanobodies we isolated are unique with its differential sensitivities to CD9 expressed on various cell types, endogenous and exogenous expression of CD9, and the level of CD9 overexpression on the cell surface. These unique characteristics may open up new possibilities in the interrogation of CD9, tetraspanins, and other cell membrane proteins and its application in disease diagnostics and therapy.

Tetraspanins are also able to assume clusters on the cell surface, shifting between homoclustered (interaction with similar tetraspanins) and heteroclustered (interaction with other partner proteins).[37] In some cases, CD9 expression levels, as well as clustering, diminish when various types of tumor cells become malignant. Yang and colleague performed a set of experimental techniques to alter the clustering states of CD9 on the cell surface.[37] They showed that overexpression of CD9 induces the formation of homoclusters, and that an anti-CD9 antibody, C9BB, preferentially targets homoclustered CD9. Our early data seemed to show that T2C001 may behave similarly like C9BB with preference to binding to homoclustered CD9 over heteroclustered CD9. In this regard, our panel of CD9 nanobody clones may have a diagnostic advantage as they can discriminate not only the expression level of CD9 but also its clustering state.

In our study, we discovered that nanobodies targeting CD9 effectively curtail the cell-cell spread of HIV-1, irrespective of their affinity to endogenous CD9. Remarkably, T2C001, which shows a strong preference for binding to overexpressed CD9, exhibited superior effectiveness in obstructing viral release. This observation aligns with established research indicating that the assembly of HIV-1 Gag proteins promotes CD9 clustering at the sites of viral egress[38] leading us to propose that T2C001's marked inhibitory capability stems from its targeted disruption at these critical exit points (Figure S9). Additionally, the CD9-specific antibody K41 has been shown to similarly impede viral budding and release, akin to the effects observed with T2C001.[35] However, K41 uniquely induces the formation of CD9 clusters, which may either displace viral proteins or facilitate their inclusion at sites of cell-cell contact, thereby exerting a dual role in either hindering or facilitating cell-cell fusion.[39] This dual functionality underscores the complex interplay between CD9 clustering and HIV-1 spread, highlighting the necessity for more detailed investigations to unravel the intricate mechanisms governing these processes.

To date, several antibodies targeting CD9 are being developed and characterized for various curative indications in cancer, auto-immunity, and infection. For example, AT1412, a patient-derived CD9 antibody, is currently in preclinical development for treatment of B acute lymphoblastic leukemia.[40] However, besides the recently isolated nanobodies against CD9[29] used for structural studies, no CD9-directed nanobodies have been explored as a therapeutic drug. Nanobodies isolated herein offer various advantages; first, depending on the cancer type, cluster-specific CD9 nanobodies may be used (combinations thereof, or engineered as bispecific antibodies). Secondly, owing to the absence of an Fc tail, these nanobodies circumvent the risk of FcγRIIA-mediated platelet aggregation and clotting, a common concern with traditional CD9 mAb.[41] Additionally, their smaller size confers a superior ability for tumor penetration, enhancing their efficacy in targeting tumor cells. This unique combination of properties positions these CD9-targeting nanobodies as a valuable asset in both the detection and treatment of malignancies, and potentially in other areas where CD9 plays a pivotal role.

Targeting CD9 with antibodies (or nanobodies) as it relates to diseases may be the best strategy over gene-based knockdown or knockout, as antibody treatment has been shown to perturb TEMs.[3] Nanobodies can achieve similar affinities to their target than traditional full-length IgGs, plus offering several more advantages.[42] Several nanobodies targeting various epitopes on HIV-1Env have been isolated from llamas immunized with soluble versions of HIV-1 Env.[43] These nanobodies have a large range of breadth and potencies against different subtypes of HIV-1, and the addition of antibody Fc tails renders them the ability to mediate Fc effector functions.[44] Alternatively, a nanobody-based host-targeting strategy to inhibit HIV-1 infection could be an attractive addition to the HIV-1 cure toolbox. Furthermore, our data show that combination treatment of J3 nanobody and T2C002 achieved an additive potency against the inhibition of HIV-1 replication. Therefore, a bispecific construct of these two clones could be an interesting next step in testing their potential therapeutic use, with or without the presence of an IgG Fc tail. This bispecific molecule can then co-engage both a viral antigen and host protein simultaneously.

Our study is limited by the lack of structural data to determine the exact binding epitopes of the nanobodies clones, the specific cell subpopulation they seemed to bind to, and their interaction with protein partners on the cell surface. Furthermore, super-resolution microscopy study may offer a closer look into the presence and formation of tetraspanin clusters to confirm our hypothesis that our nanobodies do indeed detect CD9 clustering. Lastly, we did not determine the exact mechanism of inhibition of these nanobodies, which may be different between T cells and macrophages, as well as other HIV-1 infection models.

In summary, our study successfully isolated and characterized a novel set of CD9-directed nanobodies, each exhibiting unique biophysical characteristics. These nanobodies, with their diverse properties, show promise for applications in diagnostic and therapeutic contexts across various fields. In the context of HIV-1, CD9-targeting nanobodies could be a promising host-targeting strategy to inhibit viral replication in addition to virus targeting strategies.

Limitations of the study

This study is limited by the lack of several biochemical characterization including epitope mapping, stability studies, etc. Furthermore, the structure of the nanobodies binding to CD9 could further deepen our understanding of the mechanism of action of these novel CD9 nanobodies. Additionally, although our main focus is the therapeutic efficacy of these nanobodies against HIV-1 replication, the potential role of these nanobodies in cancer, extracellular vesicle biology, and other relevant fields was under explored.

RESOURCE AVAILABILITY

Lead contact

Further information and requests for resources and reagents should be directed to and will be fulfilled by the lead contact, Dr. Steven W. de Taeye (s.w.detaeye@amsterdamumc.nl).

Materials availability

Further information and requests for resources and reagents should be directed to and will be fulfilled by the lead contact Dr. Steven W. de Taeye (s.w.detaeye@amsterdamumc.nl).

Data and code availability

- The data supporting the findings of the study are available from the corresponding author upon reasonable request.
- This paper does not report original code.
- Any additional information required to reanalyze the data reported in the paper is available from the lead contact upon request.

ACKNOWLEDGMENTS

We would like to thank Ana Alcala for support in our tissue culture work, Meliwati Poniman for providing reagents and technical support, Judith Burger for BSL-3 technical support, Mathieu Claireux and Gius Kerster for help with experimental design and analysis, and Laura Graus for visualization and flow cytometry help. We would also like to thank the administrative support in our group, Margreet Bakker and Jeroen van Wamel. Thank you to Alex Rooker and Dr. Rosalie Luiten for providing the cancer cell lines. Thank you to Joan Capella-Pujol for providing CD81-Fc. We also acknowledge the assistance of QvQ technicians for the production of nanobodies. J.C.U. is supported by TKI-PPP grants Target2Cure by Health Holland/Aidsfonds (LSHM19101-SGF) and Innovation Exchange Amsterdam (2019-1167). S.W.d.T. is supported by Young investigator grant P-53301 Aidsfonds and the amfAR's 2023 Mathilde Krim Fellowship (110425-73-RKRL).

AUTHOR CONTRIBUTIONS

Conceptualization, N.A.K., M.J.v.G., S.W.d.T., J.C.U., and R.H.; funding acquisition, N.A.K., M.J.v.G., and T.B.H.G.; supervision, N.A.K., M.J.v.G., T.B.H.G., R.H., and E.H.-C.; manuscript writing, J.C.U. and S.W.d.T.; editing, N.A.K., M.J.v.G., S.W.d.T., J.C.U., R.H., P.Z.K., S.M., T.A., G.D., and T.B.H.G.; experiments and methods, J.C.U., S.W.d.T., P.Z.K., S.M., T.A., and K.A.v.D.; revisions, J.C.U., P.Z.K., S.M., and S.W.d.T. All authors contributed to the manuscript and approved the submitted version.

DECLARATION OF INTERESTS

The authors declare no competing interests.

STAR★METHODS

Detailed methods are provided in the online version of this paper and include the following:

- KEY RESOURCES TABLE
- EXPERIMENTAL MODEL AND STUDY PARTICIPANT DETAILS
  - Cell lines
  - Isolation and culture of monocyte
- METHOD DETAILS
  - Antigen design, cloning, and production
  - Llama immunization, phage-display and periplasmic fractions
  - Production and purification of nanobodies
  - SDS PAGE/Western Blot
  - Binding ELISA
  - CA-p24 ELISA
  - CD9 overexpression
  - In silico modeling and sequence alignment
  - Biolayer interferometry (BLI)
  - Flow cytometry
  - Virus production
  - TZM-bl assay
  - Syncytium assay
  - Monocyte-derived macrophage infection
- QUANTIFICATION AND STATISTICAL ANALYSIS

SUPPLEMENTAL INFORMATION

Supplemental information can be found online at https://doi.org/10.1016/j.isci.2024.110958.

Received: April 29, 2024
Revised: August 5, 2024
Accepted: September 10, 2024
Published: September 13, 2024

REFERENCES

1. Umotoy, J.C., and de Taeye, S.W. (2021). Antibody Conjugates for Targeted Therapy Against HIV-1 as an Emerging Tool for HIV-1 Cure. Front. Immunol. *12*, 708806. https://doi.org/10.3389/fimmu.2021.708806.
2. Florin, L., and Lang, T. (2018). Tetraspanin assemblies in virus infection. Front. Immunol. *9*, 1140–1149. https://doi.org/10.3389/fimmu.2018.01140.
3. Hemler, M.E. (2008). Targeting of tetraspanin proteins–potential benefits and strategies. Nat. Rev. Drug Discov. *7*, 747–758. https://doi.org/10.1038/nrd2659.
4. Monk, P.N., and Partridge, L.J. (2012). Tetraspanins: gateways for infection. Infect. Disord.: Drug Targets *12*, 4–17. https://doi.org/10.2174/187152612798994957.
5. Reyes, R., Cardeñes, B., Machado-Pineda, Y., and Cabañas, C. (2018). Tetraspanin CD9: A Key Regulator of Cell Adhesion in the Immune System. Front. Immunol. *9*, 863. https://doi.org/10.3389/fimmu.2018.00863.
6. Kaji, K., Oda, S., Shikano, T., Ohnuki, T., Uematsu, Y., Sakagami, J., Tada, N., Miyazaki, S., and Kudo, A. (2000). The gamete fusion process is defective in eggs of Cd9-deficient mice. Nat. Genet. *24*, 279–282. https://doi.org/10.1038/73502.
7. Le Naour, F., Rubinstein, E., Jasmin, C., Prenant, M., and Boucheix, C. (2000). Severely reduced female fertility in CD9-deficient mice. Science *287*, 319–321. https://doi.org/10.1126/science.287.5451.319.
8. Löffler, S., Lottspeich, F., Lanza, F., Azorsa, D.O., Ter Meulen, V., and Schneider-Schaulies, J. (1997). CD9, a tetraspan transmembrane protein, renders cells susceptible to canine distemper virus. J. Virol. *71*, 42–49. https://doi.org/10.1128/jvi.71.1.42-49.1997.
9. Earnest, J.T., Hantak, M.P., Park, J.-E., and Gallagher, T. (2015). Coronavirus and Influenza Virus Proteolytic Priming Takes Place in Tetraspanin-Enriched Membrane Microdomains. J. Virol. *89*, 6093–6104. https://doi.org/10.1128/JVI.00543-15.
10. Earnest, J.T., Hantak, M.P., Li, K., McCray, P.B., Perlman, S., and Gallagher, T. (2017). The tetraspanin CD9 facilitates MERS-coronavirus entry by scaffolding host cell receptors and proteases. PLoS Pathog. *13*, e1006546. https://doi.org/10.1371/journal.ppat.1006546.

11. Mikuličić, S., Fritzen, A., Scheffer, K., Strunk, J., Cabañas, C., Sperrhacke, M., Reiss, K., and Florin, L. (2020). Tetraspanin CD9 affects HPV16 infection by modulating ADAM17 activity and the ERK signalling pathway. Med. Microbiol. Immunol. *209*, 461–471. https://doi.org/10.1007/s00430-020-00671-5.
12. Ovalle, S., Gutiérrez-López, M.D., Monjas, A., and Cabañas, C. (2007). Implication of the tetraspanin CD9 in the immune system and cancer. Inmunologia *26*, 65–72. https://doi.org/10.1016/S0213-9626(07)70076-8.
13. Wright, M.D., Moseley, G.W., and van Spriel, A.B. (2004). Tetraspanin microdomains in immune cell signalling and malignant disease. Tissue Antigens *64*, 533–542. https://doi.org/10.1111/j.1399-0039.2004.00321.x.
14. Thali, M. (2009). The roles of tetraspanins in HIV-1 replication. Curr. Top. Microbiol. Immunol. *339*, 85–102. https://doi.org/10.1007/978-3-642-02175-6_5.
15. Garcia, E., Nikolic, D.S., and Piguet, V. (2008). HIV-1 Replication in Dendritic Cells Occurs Through a Tetraspanin-Containing Compartment Enriched in AP-3. Traffic *9*, 200–214. https://doi.org/10.1111/j.1600-0854.2007.00678.x.
16. Grigorov, B., Attuil-Audenis, V., Perugi, F., Nedelec, M., Watson, S., Pique, C., Darlix, J.-L., Conjeaud, H., and Muriaux, D. (2009). A role for CD81 on the late steps of HIV-1 replication in a chronically infected T cell line. Retrovirology *6*, 28. https://doi.org/10.1186/1742-4690-6-28.
17. Jolly, C., and Sattentau, Q.J. (2007). Human immunodeficiency virus type 1 assembly, budding, and cell-cell spread in T cells take place in tetraspanin-enriched plasma membrane domains. J. Virol. *81*, 7873–7884. https://doi.org/10.1128/JVI.01845-06.
18. Krementsov, D.N., Rassam, P., Margeat, E., Roy, N.H., Schneider-Schaulies, J., Milhiet, P.-E., and Thali, M. (2010). HIV-1 Assembly Differentially Alters Dynamics and Partitioning of Tetraspanins and Raft Components. Traffic *11*, 1401–1414. https://doi.org/10.1111/j.1600-0854.2010.01111.x.
19. Nydegger, S., Khurana, S., Krementsov, D.N., Foti, M., and Thali, M. (2006). Mapping of tetraspanin-enriched microdomains that can function as gateways for HIV-1. J. Cell Biol. *173*, 795–807. https://doi.org/10.1083/jcb.200508165.
20. Von Lindern, J.J., Rojo, D., Grovit-Ferbas, K., Yeramian, C., Deng, C., Herbein, G., Ferguson, M.R., Pappas, T.C., Decker, J.M., Singh, A., et al. (2003). Potential Role for CD63 in CCR5-Mediated Human Immunodeficiency Virus Type 1 Infection of Macrophages. J. Virol. *77*, 3624–3633. https://doi.org/10.1128/JVI.77.6.3624-3633.2003.
21. Sato, K., Aoki, J., Misawa, N., Daikoku, E., Sano, K., Tanaka, Y., and Koyanagi, Y. (2008). Modulation of Human Immunodeficiency Virus Type 1 Infectivity through Incorporation of Tetraspanin Proteins. J. Virol. *82*, 1021–1033. https://doi.org/10.1128/JVI.01044-07.
22. Haller, C., Müller, B., Fritz, J.V., Lamas-Murua, M., Stolp, B., Pujol, F.M., Keppler, O.T., and Fackler, O.T. (2014). HIV-1 Nef and Vpu Are Functionally Redundant Broad-Spectrum Modulators of Cell Surface Receptors, Including Tetraspanins. J. Virol. *88*, 14241–14257. https://doi.org/10.1128/JVI.02333-14.
23. Lambelé, M., Koppensteiner, H., Symeonides, M., Roy, N.H., Chan, J., Schindler, M., and Thali, M. (2015). Vpu Is the Main Determinant for Tetraspanin Downregulation in HIV-1-Infected Cells. J. Virol. *89*, 3247–3255. https://doi.org/10.1128/JVI.03719-14.
24. Kruize, Z., Jim, V.C., Martinez, F.O., Di, R., Dort, K.A.V., Nuenen, A.C.V., Booiman, T., and Kootstra, N.A. (2021). CD9 and ITGA3 are regulated during HIV-1 infection in macrophages to support viral replication. Virology *562*, 9–18. https://doi.org/10.1016/j.virol.2021.07.002.
25. Umeda, R., Satouh, Y., Takemoto, M., Nakada-Nakura, Y., Liu, K., Yokoyama, T., Shirouzu, M., Iwata, S., Nomura, N., Sato, K., et al. (2020). Structural insights into tetraspanin CD9 function. Nat. Commun. *11*, 1606–1607. https://doi.org/10.1038/s41467-020-15459-7.
26. Vincke, C., and Muyldermans, S. (2012). Introduction to Heavy Chain Antibodies and Derived Nanobodies. In Single Domain Antibodies Methods in Molecular Biology, D. Saerens and S. Muyldermans, eds. (Humana Press), pp. 15–26. https://doi.org/10.1007/978-1-61779-968-6_2.
27. Hanke, L., Sheward, D.J., Pankow, A., Vidakovics, L.P., Karl, V., Kim, C., Urgard, E., Smith, N.L., Astorga-Wells, J., Ekström, S., et al. (2022). Multivariate mining of an alpaca immune repertoire identifies potent cross-neutralizing SARS-CoV-2 nanobodies. Sci. Adv. *8*, eabm0220. https://doi.org/10.1126/sciadv.abm0220.
28. Chumbe, A., Grobben, M., Capella-Pujol, J., Koekkoek, S.M., Zon, I., Slamanig, S., Merat, S.J., Beaumont, T., Sliepen, K., Schinkel, J., and van Gils, M.J. (2024). A panel of hepatitis C virus glycoproteins for the characterization of antibody responses using antibodies with diverse recognition and neutralization patterns. Virus Res. *341*, 199308. https://doi.org/10.1016/j.virusres.2024.199308.
29. Neviani, V., van Deventer, S., Wörner, T.P., Xenaki, K.T., van de Waterbeemd, M., Rodenburg, R.N.P., Wortel, I.M.N., Kuiper, J.K., Huisman, S., Granneman, J., et al. (2020). Site-specific functionality and tryptophan mimicry of lipidation in tetraspanin CD9. FEBS J. *287*, 5323–5344. https://doi.org/10.1111/febs.15295.
30. Oosterheert, W., Xenak, K.T., Neviani, V., Pos, W., Doulkeridou, S., Manshande, J., Pearce, N.M., Kroon-Batenburg, L.M.J., Lutz, M., Van Bergen En Henegouwen, P.M.P., et al. (2020). Implications for tetraspanin-enriched microdomain assembly based on structures of CD9 with EWI-F. Life Sci. Alliance *3*, 1–16. https://doi.org/10.26508/LSA.202000883.
31. Herr, M.J., Longhurst, C.M., Baker, B., Homayouni, R., Speich, H.E., Kotha, J., and Jennings, L.K. (2014). Tetraspanin CD9 modulates human lymphoma cellular proliferation via histone deacetylase activity. Biochem. Biophys. Res. Commun. *447*, 616–620. https://doi.org/10.1016/j.bbrc.2014.04.046.
32. Wei, X., Decker, J.M., Wang, S., Hui, H., Kappes, J.C., Wu, X., Salazar-Gonzalez, J.F., Salazar, M.G., Kilby, J.M., Saag, M.S., et al. (2003). Antibody neutralization and escape by HIV-1. Nature *422*, 307–312. https://doi.org/10.1038/nature01470.
33. McCoy, L.E., Groppelli, E., Blanchetot, C., de Haard, H., Verrips, T., Rutten, L., Weiss, R.A., and Jolly, C. (2014). Neutralisation of HIV-1 cell-cell spread by human and llama antibodies. Retrovirology *11*, 83. https://doi.org/10.1186/s12977-014-0083-y.
34. De Parseval, A., Lerner, D.L., Borrow, P., Willett, B.J., and Elder, J.H. (1997). Blocking of feline immunodeficiency virus infection by a monoclonal antibody to CD9 is via inhibition of virus release rather than interference with receptor binding. J. Virol. *71*, 5742–5749. https://doi.org/10.1128/jvi.71.8.5742-5749.1997.
35. Khurana, S., Krementsov, D.N., De Parseval, A., Elder, J.H., Foti, M., and Thali, M. (2007). Human Immunodeficiency Virus Type 1 and Influenza Virus Exit via Different Membrane Microdomains. J. Virol. *81*, 12630–12640. https://doi.org/10.1128/JVI.01255-07.
36. Schmid, E., Zurbriggen, A., Gassen, U., Rima, B., Ter Meulen, V., and Schneider-Schaulies, J. (2000). Antibodies to CD9, a Tetraspan Transmembrane Protein, Inhibit Canine Distemper Virus-Induced Cell-Cell Fusion but Not Virus-Cell Fusion. J. Virol. *74*, 7554–7561. https://doi.org/10.1128/JVI.74.16.7554-7561.2000.
37. Yang, X.H., Kovalenko, O.V., Kolesnikova, T.V., Andzelm, M.M., Rubinstein, E., Strominger, J.L., and Hemler, M.E. (2006). Contrasting Effects of EWI Proteins, Integrins, and Protein Palmitoylation on Cell Surface CD9 Organization. J. Biol. Chem. *281*, 12976–12985. https://doi.org/10.1074/jbc.M510617200.
38. Dahmane, S., Doucet, C., Le Gall, A., Chamontin, C., Dosset, P., Murcy, F., Fernandez, L., Salas, D., Rubinstein, E., Mougel, M., et al. (2019). Nanoscale organization of tetraspanins during HIV-1 budding by correlative dSTORM/AFM. Nanoscale *11*, 6036–6044. https://doi.org/10.1039/C8NR07269H.
39. Singethan, K., Müller, N., Schubert, S., Lüttge, D., Krementsov, D.N., Khurana, S.R., Krohne, G., Schneider-Schaulies, S., Thali, M., and Schneider-Schaulies, J. (2008). CD9 Clustering and Formation of Microvilli Zippers Between Contacting Cells Regulates Virus-Induced Cell Fusion. Traffic *9*, 924–935. https://doi.org/10.1111/j.1600-0854.2008.00737.x.
40. Schotte, R., Villaudy, J., De Jong, G., Neviani, V., Pos, W., Levie, S.E., Go, D.M., Yasuda, E., Frankin, E., Cercel, M., et al. (2020). Preclinical Development of AT1412, a Patient Derived CD9 Antibody That Does Not Induce Thrombosis for Treatment of B ALL. Blood *136*, 41–42. https://doi.org/10.1182/blood-2020-134088.
41. Worthington, R.E., Carroll, R.C., and Boucheix, C. (1990). Platelet activation by CD9 monoclonal antibodies is mediated by the $F_{C\gamma}$ II receptor. Br. J. Haematol. *74*, 216–222. https://doi.org/10.1111/j.1365-2141.1990.tb02568.x.
42. Yang, E.Y., and Shah, K. (2020). Nanobodies: Next Generation of Cancer Diagnostics and Therapeutics. Front. Oncol. *10*, 1182. https://doi.org/10.3389/fonc.2020.01182.
43. Weiss, R.A., and Verrips, C.T. (2019). Nanobodies that Neutralize HIV. Vaccines *7*, 77. https://doi.org/10.3390/vaccines7030077.
44. Schriek, A.I., Van Haaren, M.M., Poniman, M., Dekkers, G., Bentlage, A.E.H., Grobben, M., Vidarsson, G., Sanders, R.W., Verrips, T., Geijtenbeek, T.B.H., et al. (2022). Anti-HIV-1 Nanobody-IgG1 Constructs With Improved Neutralization Potency and the Ability to Mediate Fc Effector Functions. Front. Immunol. *13*, 893648. https://doi.org/10.3389/fimmu.2022.893648.
45. Capella-Pujol, J., De Gast, M., Radić, L., Zon, I., Chumbe, A., Koekkoek, S., Olijhoek, W., Schinkel, J., Van Gils, M.J., Sanders, R.W., and Sliepen, K. (2023). Signatures of VH1-69-derived hepatitis C virus neutralizing

antibody precursors defined by binding to envelope glycoproteins. Nat. Commun. *14*, 4036. https://doi.org/10.1038/s41467-023-39690-0.

46. De Haard, H.J.W., Bezemer, S., Ledeboer, A.M., Müller, W.H., Boender, P.J., Moineau, S., Coppelmans, M.-C., Verkleij, A.J., Frenken, L.G.J., and Verrips, C.T. (2005). Llama Antibodies against a Lactococcal Protein Located at the Tip of the Phage Tail Prevent Phage Infection. J. Bacteriol. *187*, 4531–4541. https://doi.org/10.1128/JB.187.13.4531-4541.2005.
47. Hoogenboom, H.R., Griffiths, A.D., Johnson, K.S., Chiswell, D.J., Hudson, P., and Winter, G. (1991). Multi-subunit proteins on the surface of filamentous phage: methodologies for displaying antibody (Fab) heavy and light chains. Nucleic Acids Res. *19*, 4133–4137. https://doi.org/10.1093/nar/19.15.4133.
48. Gangaiah, D., Ryan, V., Van Hoesel, D., Mane, S.P., Mckinley, E.T., Lakshmanan, N., Reddy, N.D., Dolk, E., and Kumar, A. (2022). Recombinant *Limosilactobacillus* (*Lactobacillus*) delivering nanobodies against *Clostridium perfringens* NetB and alpha toxin confers potential protection from necrotic enteritis. MicrobiologyOpen *11*, e1270. https://doi.org/10.1002/mbo3.1270.
49. Marks, J.D., Hoogenboom, H.R., Bonnert, T.P., McCafferty, J., Griffiths, A.D., and Winter, G. (1991). By-passing immunization. J. Mol. Biol. *222*, 581–597. https://doi.org/10.1016/0022-2836(91)90498-U.
50. Struijf, E.M., De La O Becerra, K.I., Ruyken, M., De Haas, C.J.C., Van Oosterom, F., Siere, D.Y., Van Keulen, J.E., Heesterbeek, D.A.C., Dolk, E., Heukers, R., et al. (2023). Inhibition of cleavage of human complement component C5 and the R885H C5 variant by two distinct high affinity anti-C5 nanobodies. J. Biol. Chem. *299*, 104956. https://doi.org/10.1016/j.jbc.2023.104956.
51. Molina, M.A., Vink, M., Berkhout, B., and Herrera-Carrillo, E. (2023). In-house ELISA protocols for capsid p24 detection of diverse HIV isolates. Virol. J. *20*, 269. https://doi.org/10.1186/s12985-023-02242-5.
52. Tersmette, M., Winkel, I.N., Groenink, M., Gruters, R.A., Spence, R.P., Saman, E., Van Der Groen, G., Miedema, F., and Huisman, J.G. (1989). Detection and subtyping of HIV-1 isolates with a panel of characterized monoclonal antibodies to HIV p24gag. Virology *171*, 149–155. https://doi.org/10.1016/0042-6822(89)90521-7.
53. Dunbar, J., Krawczyk, K., Leem, J., Marks, C., Nowak, J., Regep, C., Georges, G., Kelm, S., Popovic, B., and Deane, C.M. (2016). SAbPred: a structure-based antibody prediction server. Nucleic Acids Res. *44*, W474–W478. https://doi.org/10.1093/nar/gkw361.
54. Meng, E.C., Goddard, T.D., Pettersen, E.F., Couch, G.S., Pearson, Z.J., Morris, J.H., and Ferrin, T.E. (2023). UCSF ChimeraX : Tools for structure building and analysis. Protein Sci. *32*, e4792. https://doi.org/10.1002/pro.4792.
55. Okonechnikov, K., Golosova, O., and Fursov, M.; UGENE team (2012). Unipro UGENE: a unified bioinformatics toolkit. Bioinformatics *28*, 1166–1167. https://doi.org/10.1093/bioinformatics/bts091.
56. Sievers, F., Wilm, A., Dineen, D., Gibson, T.J., Karplus, K., Li, W., Lopez, R., McWilliam, H., Remmert, M., Söding, J., et al. (2011). Fast, scalable generation of high-quality protein multiple sequence alignments using Clustal Omega. Mol. Syst. Biol. *7*, 539. https://doi.org/10.1038/msb.2011.75.
57. Herrera-Carrillo, E., Paxton, W.A., and Berkhout, B. (2014). The search for a T cell line for testing novel antiviral strategies against HIV-1 isolates of diverse receptor tropism and subtype origin. J. Virol. Methods *203*, 88–96. https://doi.org/10.1016/j.jviromet.2014.03.021.
58. Derking, R., Allen, J.D., Cottrell, C.A., Sliepen, K., Seabright, G.E., Lee, W.-H., Aldon, Y., Rantalainen, K., Antanasijevic, A., Copps, J., et al. (2021). Enhancing glycan occupancy of soluble HIV-1 envelope trimers to mimic the native viral spike. Cell Rep. *35*, 108933. https://doi.org/10.1016/j.celrep.2021.108933.
59. Peden, K., Emerman, M., and Montagnier, L. (1991). Changes in growth properties on passage in tissue culture of viruses derived from infectious molecular clones of HIV-1LAI, HIV-1MAL, and HIV-1ELI. Virology *185*, 661–672. https://doi.org/10.1016/0042-6822(91)90537-l.
60. Wu, X., Parast, A.B., Richardson, B.A., Nduati, R., John-Stewart, G., Mbori-Ngacha, D., Rainwater, S.M.J., and Overbaugh, J. (2006). Neutralization escape variants of human immunodeficiency virus type 1 are transmitted from mother to infant. J. Virol. *80*, 835–844. https://doi.org/10.1128/JVI.80.2.835-844.2006.
61. Sanders, R.W., Derking, R., Cupo, A., Julien, J.P., Yasmeen, A., de Val, N., Kim, H.J., Blattner, C., de la Peña, A.T., Korzun, J., et al. (2013). A Next-Generation Cleaved, Soluble HIV-1 Env Trimer, BG505 SOSIP.664 gp140, Expresses Multiple Epitopes for Broadly Neutralizing but Not Non-Neutralizing Antibodies. PLoS Pathog. *9*, e1003618. https://doi.org/10.1371/journal.ppat.1003618.
62. McCoy, L.E., Quigley, A.F., Strokappe, N.M., Bulmer-Thomas, B., Seaman, M.S., Mortier, D., Rutten, L., Chander, N., Edwards, C.J., Ketteler, R., et al. (2012). Potent and broad neutralization of HIV-1 by a llama antibody elicited by immunization. J. Exp. Med. *209*, 1091–1103. https://doi.org/10.1084/jem.20112655.
63. Lifson, J.D. (1993). [1] Fusion of human immunodeficiency virus-infected cells with uninfected cells. Methods Enzymol. *221*, 3–12. https://doi.org/10.1016/0076-6879(93)21003-Q.

STAR★METHODS

KEY RESOURCES TABLE

REAGENT or RESOURCE	SOURCE	IDENTIFIER
Antibodies		
Anti-CD9 monoclonal antibody	Sino Biological	Cat# 10626-MM07; RRID: AB_2860324
CD9 Antibody PerCPcy5.5	BioLegend	Cat# 312109; RRID: AB_2728250
CD9 Antibody	AbCam	Cat# ab223052
HRP-conjugated anti-mouse IgG	SeraCare	Cat# 5220-0330
HRP Streptavidin	BioLegend	Cat# 405210
Goat anti-llama IgG-HRP	Abcam	Cat# ab112786
Anti-VHH rabbit antibody (clone QE19)	QVQ B.V.	
Donkey anti-rabbit-HRP	Jackson ImmunoResearch	Cat# 711-035-152
MonoRab™ Rabbit Anti-Camelid VHH-HRP	GenScript	Cat# A02018
PerCPCy5.5-conjugated anti-CD9 antibody	BioLegend	Cat# 312115
Bacterial and virus strains		
E. coli TG1	Invitrogen	Cat# C303003
Rosetta 2 (DE3) BL21 cells	Merck	Cat# 71400-3
HIV LAI, BG505, NL4-3 BaL	NIH HIV Reagent Program	N/A
Biological samples		
Buffy coats from healthy donors	Sanquin Dutch national blood bank	N/A
Monocytes	Obtained from blood donors	N/A
Chemicals, peptides, and recombinant proteins		
DTT (Dithiothreitol)	Thermo Fisher Scientific	Cat# R0861
O-phenylenediamine dihydrochloride (OPD)	Sigma-Aldrich	Cat# P8787
TMB substrate	Sigma-Aldrich	Cat# T0440
Ni-NTA resin	Thermo Fisher Scientific	Cat# 88221
Strep-Tactin resin	IBA Lifesciences	Cat# 2-1206-025
Superdex 200 column	Cytiva	Cat# 28-9909-44
PEI MAX	Polysciences	Cat# 24765
Triethanolamine	Sigma-Aldrich	Cat# T1502
DEAE-Dextran	Sigma-Aldrich	Cat# D9885
2-mercaptoethylamine (2-MEA)	Sigma-Aldrich	Cat# M9768-25G
Ni-NTA agarose	Qiagen	Cat# 30210
Ni-NTA ELISA Plates	Qiagen	Cat# 35061
Tris	Sigma-Aldrich	Cat# T7943
Fetal bovine serum	R&D Biosystems	Cat# S11150H
Penicillin-Streptomycin (5,000 U/mL)	Gibco	Cat# 15070063
EDTA (Titriplex III)	Sigma-Aldrich	Cat# 1084180100
PBS	Thermo Fisher Scientific	Cat# 10010023
Vivaspin 20 3K, 5K, 100K Da MWCO, polyethersulfone	Sigma-Aldrich	Cat# GE28-9322
Marvel Milk Powder	Tesco	
Milk powder	PanReac AppliChem	Cat# A0830

(*Continued on next page*)

Continued

REAGENT or RESOURCE	SOURCE	IDENTIFIER
Critical commercial assays		
HIV-1 Gag p24 DuoSet ELISA kit	R&D Biosystems	Cat# DY7360-05
Multiskan Go plate reader	Thermo Fisher Scientific	
ImageQuant LAS 4000	Cytiva	28-9893-96
SPECTROstar Nano	BMG Labtech	N/A
Glomax Microplate Reader	Promega	GM3000
Dynapro Nanostar	Wyatt Technology	N/A
Octet K2 system	Sartorius	N/A
Octet Ni-NTA Biosensors	Sartorius	18–5101
FACSymphony A1 Cell Analyzer	BD Biosciences	N/A
Lumi-Phos HRP	Lumigen	Cat# PSA-100
Experimental models: Cell lines		
HEK-293F cells	Thermo Fisher	Cat# R79007
HEK293T cells	ATCC	Cat# CRL-11268
TZM-bl cells	NIH HIV Reagent Program	Cat# 8129
THP-1, Raji, SupT1 cells	ATCC	Cat# CRL-1942, CCL-86
HeLa cells	ATCC	Cat# CCL-2
Recombinant DNA		
Codon-optimized full-length CD9 gene fragment	IDT	Custom
pCI-neo vector	Promega	Cat# E1841
pUC19 vector	Thermo Fisher Scientific	Cat# SM0312
pPQ81 vector (phagemid)	Custom (derived from pHEN1)	Custom
pEQ22 vector (derived from pMEK222)	Custom	Custom
Software and algorithms		
GraphPad Prism 9	GraphPad Software	Custom license
UGENE software	Custom	Free software
Clustal Omega	Custom	Free software
ChimeraX	UCSF	Free software
Zotero		
Alphafold		
Other		
Lipofectamine 2000	Invitrogen	Cat# 11668019
Opti-MEM	Thermo Fisher Scientific	Cat# 31985070
FreeStyle 293 Expression medium	Thermo Fisher Scientific	Cat# 12338018
RPMI 1640 Medium	Gibco	Cat# 11875093
DMEM	Gibco	Cat# 11965092
Steritop 0.22 μm filter	Merck Millipore	Cat# SCGPT05RE
Ficoll-Isopaque	Sigma-Aldrich	Cat# GE17-1440-02
Amicon 10 MWCO filters	Millipore Sigma	Cat# UFC901024
Nunc Maxisorp plates	Thermo Fisher Scientific	Cat# VWR 735-0083
Novex Wedgewell 10–20% Tris-Glycine gels	Invitrogen	Cat# XP10200BOX
QuikChange Site-Directed Mutagenesis Kit	New England Biolabs	Cat# E0554S
NEBNext® High-Fidelity 2× PCR Master Mix	New England Biolabs	Cat# M0541S

(*Continued on next page*)

Continued

REAGENT or RESOURCE	SOURCE	IDENTIFIER
96-well Half Area ELISA Microplates - Clear	Greiner Bio-One	Cat# 11990657
96-well Half Area ELISA Microplates - White	Greiner Bio-One	Cat# 655074
Bovine serum albumin (BSA)	VWR	Cat# 422361

EXPERIMENTAL MODEL AND STUDY PARTICIPANT DETAILS

Cell lines

Cells are handled and maintained following ATCC recommendations. Briefly, HEK293T cells are maintained in Dulbecco's Modified Eagle's Medium (DMEM) supplemented with 10% heat-inactivated Fetal Bovine Serum (FBS), 2 mM L-glutamine, and 1% Penicillin-Streptomycin (P/S). THP-1, and Raji cells are maintained in RPMI-1640 Medium supplemented with 10% FBS and 1% P/S. SupT1 cells were maintained in Advanced RPMI supplemented (Thermo Fisher Scientific) with 1% L-glutamine, P/S, and 3% FBS. For subculturing of adherent cells, 0.05% w/v of Trypsin/EDTA solution was used to detach cells from the flasks. The cell lines were authenticated visually by checking the morphology of cells by microscope following ATCC guidelines.

Isolation and culture of monocyte

Monocytes were obtained from buffy coats from healthy blood donors as described previously[24] (Sanquin Dutch national blood bank). First, PBMCs were isolated from buffy coats using Ficoll-Isopaque density gradient centrifugation. Monocytes were then isolated by adherence to plastic, and cultured in Iscove's modified Dulbecco's medium (IMDM; Lonza, Basel, Switzerland) supplemented with 10% heat-inactivated human pooled serum (HPS; Sanquin Dutch national blood bank, Amsterdam, Netherlands), penicillin (100 U/mL; Invitrogen, Waltham, MA, USA), and streptomycin (100 mg/mL; Invitrogen) (IMDM complete) for 5 days at 37°C in a humidified 5% CO_2 incubator to allow differentiation into monocyte-derived macrophages (MDM).

METHOD DETAILS

Antigen design, cloning, and production

A gene fragment encoding a codon-optimized full length CD9 sequence, CD5 signal peptide, flanked by *XhoI* and *NotI* restriction sequences was purchased from IDT. The gene fragment was cloned into pCI-neo (Promega) via restriction digestion and subsequently ligated. Sequence alignment was confirmed by DNA sequencing (Macrogen). For the soluble fragment of CD9, amino acids 112–195 corresponding to the large extracellular loop (LEL), were purchased as a gene fragment and cloned in pUC19 vector containing an N-terminal signal peptide, and a C-term 6xHis or Strep-TagII for purification.

Soluble CD9 LEL was expressed in HEK-293F (Invitrogen), maintained in Freestyle medium (Life technologies). Briefly, a 1:3 ratio of DNA:PEI MAX (Polysciences) combined in Opti-MEM (Thermo Fisher Scientific) was used to transfect HEK293F cells, and culture supernatant was harvested after 5 to 6 days of incubation at 37°C in a humidified CO_2 shaking incubator. Supernatant was harvested by centrifugation and filtered using 0.22 μm Steritop filters (Merck Millipore) prior to Ni-NTA or StrepTactin purification as previously described.[45] Proteins were buffer-exchanged with a 10 MWCO Amicon filter followed by size exclusion chromatography using Superdex 200 (Cytiva).

Llama immunization, phage-display and periplasmic fractions

Two *Llama Glama* (Amy and Gary) were immunized with purified recombinant CD9 LEL. Both animals were immunized twice with 100 μg CD9 LEL at day 0 and day 14, followed by two immunizations of 50 μg CD9 LEL at day 28 and day 35. Serum samples from days 0, 28, and 50 were collected to test the humoral immune response. RNA was extracted from llama peripheral blood mononuclear cells (PBMC) isolated from whole blood drawn at day 50 for nanobody phage library construction according to standard protocols.[46] Nanobody-encoding genes were cloned into a phagemid pPQ81 vector (derived from pHEN1) to generate phage display libraries.[47] To select for CD9-reactive nanobodies, phages were produced and used in two subsequent rounds of biopanning according to standard procedures.[48,49] Biopanning was performed at room temperature (RT) and all incubation steps are under continuous shaking, unless stated otherwise. CD9 LEL was coated overnight (O/N) at different concentrations (round 1: 500 ng/well and 50 ng/well, round 2: 500 ng/well, 50 ng/well and 5 ng/well) on Nunc Maxisorp plates (Thermo Fisher Scientific) at 4°C, without shaking. Wells and phages were pre-blocked with either 4% or 2% skimmed milk, respectively, and phages (round 1: $\sim 10^{10}$ CFU/well, round 2: $\sim 10^{8}$ CFU/well) were incubated for 2 h on the coated wells. Subsequently, wells were washed extensively to remove unbound phages. Phages were eluted with triethanolamine solution (TAE, pH > 10) for 15 min, and rescued by infection in *E. coli* TG1 bacteria. Nanobodies were expressed in the *E. coli* periplasm using IPTG induction for 4 h. Freeze and thawing of the bacterial pellets was used to collect periplasmic fractions.

Production and purification of nanobodies

Nanobody sequences were cloned into pPQ81 vectors including a C-terminal Myc- and 6x His-tag or into pEQ22 (pMEK222) expression vector including a C-terminal FLAG- and 6xHis-tag for detection and purification. Nanobodies were produced in *E. coli* Rosetta 2 (DE3) BL21 cells (Merck) and purified using Ni-NTA as described previously.[50]

SDS PAGE/Western Blot

For protein verification, 4 μg of CD9 LEL or nanobodies were analyzed using Novex 10–20% Tris-Glycine Mini Protein gels (Thermo Fisher Scientific), stained with PageBlue Protein Staining Solution (Thermo Fisher Scientific), and using Precision Plus Protein Standard Dual Color (Biorad) as the marker. Proteins were mixed with loading dye (0.125 M Tris-Hcl pH 6.8, 20% glycerol, 4% SDS, 0.05% bromophenol blue in MQ water) with or without dithriothreitol (DTT, 50 mM), boiled at 95°C for 10 min.

CD9 LEL was electroblotted onto nitrocellulose membranes and subsequently blocked O/N in TBS-T containing 2–3% BSA. For immunodetection, anti-CD9 mAb (Sino Biological) was used following manufacturer's recommendation. For detection, HRP-conjugated anti-mouse IgG (H + L) Antibody (sera care) was diluted 1:3000. The membranes were then washed five times in TBST and the bands were visualized using the ECL system, according to the manufacturer's instructions (Pierce). Membranes were visualized using ImageQuant LAS 4000.

Binding ELISA

Nunc MaxiSorp plates (Thermo Fisher Scientific) were coated with 2 μg/mL CD9 LEL in 50 μL DPBS and incubated O/N at 4°C. Subsequently, 200 μL 4% milk-DPBS were used to block each well. In each step, nanobodies were diluted in 1% milk-DPBS and each step was followed by washing 3 times with DPBS-0.05% tween (PBS-T). To test for humoral immune response, llama sera were serially diluted 10× starting from 100× dilution and detected with goat anti-llama IgG HRP (Abcam). For periplasmic binding, 10 μL of periplasmic extracts containing nanobodies were added per well and detected with rabbit anti-VHH (clone QE19, QVQ B.V.) and donkey anti-rabbit-HRP (Jackson ImmunoResearch). Plates were developed with 3.7 mM O-phenylenediamine dihydrochloride (OPD) dissolved in substrate buffer (Na_2HPO_4 50 mM, Citric Acid 25 mM) supplemented with 0.03% H_2O_2. The reaction was stopped with 25 μL 1 M sulfuric acid. Absorbance was measured at 490 nm using a Multiskan Go plate reader (Thermo Fisher Scientific).

To determine binding affinity of purified nanobodies by ELISA, MonoRab anti-camelid VHH-HRP (Genscript) was used as the secondary antibody. HRP substrate, 3,3′,5,5′-Tetramethylbenzidine (TMB) was prepared in developing solution (0.1 M NaAc +0.1 M citric acid +1% TMB +0.01% H_2O_2). To stop the reaction, 0.8 M H_2SO_4 was added. Optical density was measured using a SPECTROstar Nano Microplate Reader (BMG LabTech) with a 450 nm filter.

CA-p24 ELISA

To quantify HIV-1 particles, the p24 capsid protein (CA-p24) production was measured with the CA-p24 ELISA using the HIV-1 Gag p24 DuoSet ELISA kit (R&D systems)[51] or with an in-house developed ELISA protocol.[52] Briefly, mouse anti-HIV-1 Gag p24 capture antibody was coated on high-binding white half-area 96-well plates (Greiner Bio-One B.V.) and 50 μL of samples/supernatant were added onto each well before the addition of biotinylated mouse anti-HIV-1 Gag p24 detection antibody. Finally, 50 μL of Strepavidin-HRP (R&D Systems) solution was added onto each well. The standard curve was prepared from the HIV-1 Gag p24 standard stock (1 μg/mL) (Aalto Bio Reagents Ltd), starting at 1.5 ng/μL serially diluted 10-fold. The fluorescence was measured by the GloMax reader (Promega, Madison, WI, USA).

CD9 overexpression

For transient expression of CD9, HEK293T cells were transfected with pCI-Neo-CD9 full length plasmid. Briefly, 4-6 × 10^6 cells were seeded in a T75 flask in complete DMEM medium and incubated O/N. The following day, a solution of 20 μg pCI-Neo-CD9 (or mock, 5 μg, 40 μg) full length were mixed with 3:1 ratio of PEI to DNA in 1.5 mL Opti-MEM and incubated for 15 min at RT. The DNA-PEI mix was added into the flask while slowly mixing. The medium was changed 24 h later with fresh complete DMEM. Transfected cells were harvested 24 h later.

In silico modeling and sequence alignment

Nanobody structure modeling was performed using Nanobuilder2[53] and visualization and analysis was performed using ChimeraX.[54] Structure of CD9 and 4C8 were acquired from RCSB PDB (PDB: 6Z1V). Multiple sequence alignments were performed, visualized, and analyzed using UGENE software and subsequently, the built-in Clustal Omega program.[55,56] CDR amino sequences were labeled according to IMGT numbering system.

Biolayer interferometry (BLI)

To determine binding kinetics of CD9 nanobodies, we used BLI. Briefly, CD9 nanobodies were immobilized onto Ni-NTA biosensor (Sartorius) in assay buffer (1× DPBS, 0.02% Tween 20, 0.1% BSA) at 1000 nM CD9 LEL was used as an analyte at varying concentration. The duration of each step (baseline, association, and dissociation) was set to 150 s. Biosensors were regenerated (1× DPBS, 10 mM glycine) and activated (1× DPBS, 10 mM NiCl2) after each round. BLI was performed using Octet K2 (ForteBio).

Flow cytometry

HEK293T cells were treated with 0.05% w/v of Trypsin/EDTA solution (Corning Inc.), washed twice in DPBS and resuspended in DPBS containing 1% BSA (FACS buffer). To determine CD9 expression, cells were stained with PerCPCy5.5-conjugated anti-CD9 antibody per manufacturer's recommendation (Biolegend). PerCPCy5.5-conjugated anti-IgG1 κ isotype (clone MOPC-21, Biolegend) was included as a control. For nanobody binding, 1×10^6 cells in 100 μL FACS buffer were incubated with nanobodies for 30 min on ice followed by MonoRab Rabbit Anti-Camelid VHH Cocktail-PE (GenScript) per manufacturer's recommendation. Washing steps with TBS-T followed each step and incubation performed on ice in the dark. At least 20,000 events were acquired on a FACS Symphony A1 (BD Biosciences).

Virus production

HIV LAI, BG505, and NL4-3 BaL were obtained through the NIH HIV reagent program. Viruses were produced by transient transfection of HEK293T cells using Lipofectamine 200 transfection reagent (Invitrogen) as previously described[57] or calcium phosphate methods.[24] For BG505.T332N, the molecular clone was designed as previously described.[58–60]

TZM-bl assay

The HIV-1 neutralization capacity of nanobodies was tested against BG505 molecular clone as previously described.[61] Briefly, one day prior to infection, TZM-bl cells per were plated on a 96-well plate at a density of 1.7×10^4 cells/well and incubated at 37°C in 5% CO_2 for 24 h. Serial dilutions of CD9-directed nanobodies or J3 control were added onto wells and incubated for 1 h before addition of virus. J3 is a highly potent nanobody that can neutralize over 90% of HIV-1 strains tested.[62] Viral stocks were supplemented with 40 mg/mL of DEAE. Three days post-infection, the cells were washed with DPBS and lysed in lysis buffer, pH 7.8 (25 mM Glycylglycine (Gly-Gly), 15 mM $MgSO_4$, 4 mM EGTA tetrasodium, 10% Triton X-). Bright-Glo kit (Promega, Madison, WI) and a Glomax Luminometer (Turner BioSystems, Sunnyvale, CA) were used to measure Luciferase activity. The infectivity of each virus without inhibitor was set at 100%.

Syncytium assay

Syncytium formation was evaluated by microscopy adapted from Lifson.[63] Briefly, 5×10^4 SupT1 cells were aliquoted per well in a 96-well flat-bottom tissue culture plates with 50 μL of CD9-directed nanobodies at different concentration and incubated for 1 h. HIV LAI at MOI of 15 was then added and incubated at 37°C until syncytia formation was observed. Syncytia is scored as follows; 6 = numerous large opaque syncytia with no viable cells to 0 = 100% viable cells with no syncytia formation. At 36 h post-infection, when the reference control (virus and cell only wells) has visible syncytia of score 3 or 4, scoring of sample wells were performed.

Monocyte-derived macrophage infection

Monocytes were plated at a density of 100,000 cells per well in 100 μL IMDM complete and allowed to differentiate into MDM for 5 days. MDM were inoculated with HIV-1 NL4-3 Bal (MOI 0.04) and after 48 h, supernatant was aspirated and fresh medium was added to the cells. At day 3 post-infection, CD9-directed nanobodies and J3 were added to the cells. Supernatant was harvested on days 3 and 7 post-infection to determine HIV-1 replication by measuring Gag p24 production in supernatant using a protocol previously described.[52]

QUANTIFICATION AND STATISTICAL ANALYSIS

Data was analyzed using Graphpad Prism (version 9.3.1; GraphPad Software, San Diego, CA, USA). Sigmoid function in Prism software version 9 was used to determine nonlinear regression curves and to calculate 50% inhibitory concentrations (IC_{50}). Paired group-wise comparisons were performed using Friedman's ANOVA. A *p*-value of <0.05 was considered statistically significant. Nanobody/antibody EC_{50} are calculated using Graphpad Prism Non-linear fit using variable slope (four parameters).